Modeling and Simulation of a Combined Reactor/Pressure Swing Adsorption Unit for Isomerization of a Mixed Feed of Pentanes and Hexanes

Kevin F. Loughlin, Chemical Engineering., King Fahd University of Petroleum & Minerals, KFUPM Box25, Dhahran 31261, Saudi Arabia loughkf@kfupm.edu.sa and **Tareg M. Al-Soudani**, Yanbu Refinery, Saudi Aramco, Lab. Building, Room 117, Yanbu, Saudi Arabia tareq.soudani@aramco.com.

Presented in Session: 02E04 PSA/TSA AIChE National Meeting, Cincinnati, Ohio, Oct 30th -Nov 4th 2005

Abstract: A novel process for isomerizing and separating n-pentane and n-hexane to their branched isomers is proposed. Both reactor and separation units are combined in one vessel. The vessel is divided into two sections: a reactor section and a PSA separation section. The reactor section is packed with Pt/Y-zeolite catalyst. The PSA separation section is equipped with a 5A zeolite adsorbent. A dispersed plug flow mathematical model of the entire process is developed using hydrogen purge. The model is used to investigate the dynamics of the PSAR units. For a constant molar feed containing equimolar fractions of 0.03 for each of n-C_5, n-C_6, i-C_5 and i-C_6, the molar fractions of i-C_5 and i- C_6 rise to values of 0.0439 and 0.045 after reaching equilibrium conversion at the end of the reactor section. The PSA section allows for complete separation of n-C_5 and n-C_6 from the reactor section effluent stream. Both 2D and 3D plots are reported as 2D plots are found insufficient to isolate all phenomena.

1. INTRODUCTION

The concept of adsorptive reactors to achieve higher conversions in chemical reactions was originated by Vaporciyan and Kadlec in 1987 [1], and expanded in an experimental pressure swing reaction study of the catalytic oxidation of carbon monoxide with adsorption on 5A zeolite [2]. They employed a homogeneous packed bed of combined catalyst and adsorbent and most studies have followed this path. The basic premise involves shifting an equilibrium reaction to the right by adsorbing one or more of the products thus promoting the conversion. Other PSR systems that have been studied are dehydrogenation reaction of ethane [3], dehydrogenation reaction of methylcyclohexane to toluene [4], hypothetical dissociation reactions [5,6,7], steam methane reforming [8,9], total isomerization reaction [10], Claus process [11], and HCN synthesis [11]. Sircar et al reviewed the literature of PSR systems [12]. An advantage of applying these concepts is that both capital and operating cost may be minimized because the downstream separation section can be reduced or eliminated from the conventional process.

In the isomerization process of n-C_5 and n-C_6 to i-C_5 and i-C_6 homogeneous mixing of 5A adsorbent and catalyst in the PSR unit cannot be used as it is the reactant that is adsorbed. In the earlier studies, the main objective of applying the homogeneous PSR concept is to increase the conversion to a value higher than the equilibrium value by shifting the equilibrium reaction to the right. In the isomerization reaction process, however, the heterogeneous PSR concept is applied with an adsorbent bed following a catalyst bed within the same column because the main objective here is to reduce the required unit operation equipment [10]. In this study we report on the isomerization of n-C_5 and n-C_6 to i-C_5 and i-C_6 in a PSAR unit.

The proposed process flow diagram for the isomerization of n-alkanes to isoalkanes in the PSAR unit is presented in Figure 1. The unit consists of two columns with each column consisting of a catalyst-packed region followed by adsorbent packed region. The system is modeled as a non-isothermal process containing five components (n-C_5/i-C_5/n-C_6/i-C_6/H_2). The cyclic steps are shown in Figure 2:

Step 1: Pressurization/Reaction: The unit is pressurized by feeding the feedstock (at high pressure), into the column. In the catalyst bed, partial conversion of n-C_5 and n-C_6 to i-C_5 and i-C_6, respectively, takes place. There is no effluent from the unit at this step.

Step 2: Reaction/Adsorption: The high pressure feedstock is fed to the catalyst bed where partial conversion of n-C_5/n-C_6 to i-C_5/i-C_6 takes place. Then it enters the adsorbent region where unreacted n-C_5 and n-C_6 are adsorbed. The effluent from the unit, composed of i-C_5, i-C_6 and hydrogen is fed to H_2 PSA unit where i-C_5 and i-C_6 are separated and taken off as process product. H_2 is recycled to the process as purge. This step continues until the adsorbent bed reaches a specified saturation limit. Then, feed is shut off, and step 3 is introduced.

Step 3: Blowdown/Reaction: The unit is depressurized to a lower pressure level in a similar direction to that of the reaction/adsorption step. Desorption of reactive components takes place in both sections. A gas stream containing all components of the system exits the unit. Usually, this stream is considered as waste stream and discharged off in most conventional PSA processes. In a later study, this stream is reutilized.

Step 4: Desorption/Reaction: Hydrogen gas, which is considered as inert, is introduced to the reactor/adsorbent bed at low pressure This step desorbs the remaining n-C_5 and n-C_6 from the adsorbent and catalyst beds. The purge stream is introduced at both ends of the vessel simultaneously in a ratio 10 % for the reactor and 90 % for the adsorber. The waste stream is collected from the interface region.

2 THEORY

An axial dispersed PFR model is applied to describe the dynamic behavior of the PSAR unit [Table 1]. The reaction rate parameters are taken from the paper of Bryant and Spivey [13][Table 2].The main resistances to mass transfer in the adsorbent region are external fluid film resistance and macropore diffusion in series. These two resistances are combined in a global resistance according to a lumped model suggested by Morbidelli et al [14]. Gas and solids properties are assumed independent of temperature. Adsorption equilibrium is described by Nitta et al. model [15] as per Silva and Rodrigues papers [16, 17] for 5A.

$$K_{ads} = \frac{1}{P}\frac{\theta}{(1-\theta)^n} \tag{1}$$

Data for normal alkanes in Y zeolite are taken from paper of Barrer and Sutherland [18], and reevaluated for this model. The equilibrium constants for the iso alkanes on Y zeolite are assumed identical to the normal alkanes [Tables 1 & 2]. The adsorption equilibrium constant is the most sensitive temperature-dependent term, and is assumed to follow the normal exponential temperature dependence $K_{ads} = K_0 \exp[(-\Delta H_{ads})/ RT]$. Further details are given in the thesis of Al-Soudani [19].

3 RESULTS AND DISCUSSION

The cycle starts initially with clean adsorbent and a gas phase free of n-C_5, n-C_6, i-C_5 and i-C_6. The total length of the column is 100 cm. Parametric values used for simulations of conventional PSAR system are summarized in Table 3. The results of the simulation are provided on 2-dimensional plots of variables for the end of any step before moving on to the next step, and on 3-dimensional plots where the transition in each step is provided.

The velocity profiles at the end of each of the four steps are illustrated in Figure 3 and during the step transition in Figure 4. Initially, at reaction/pressurization step, the velocity at the vessel inlet is 30 times higher than its final value due to pressurization effect at constant flux [Figure 4a]. At the end of reaction/pressurization step, the inlet velocity reaches a normal linear value since all the bed at this time is pressurized [Figure 3a]. The velocity at the end of the bed is always zero since the bed is closed at the adsorber-section end during this step. The bed velocity during reaction/adsorption step quickly reaches a constant value in the reactor section identical to the inlet velocity [Figure 4b] but drops off slightly in the adsorption section due to adsorption of the normals [Figures 3a, 4b]. Because of the pressure reduction, the final velocity of the blowdown/reaction step is expected to be at least 7.5 times higher than feed velocity. The buildup to this higher value is slow as may be observed in Figure 4c.The increase in velocity, above the expected 7.5 value towards the end of the step is due to desorption of components that were adsorbed in the solid phase during the previous steps. The exit velocity at the end of this step reaches 88 times the feed velocity at the exit location [Figures 3b,4c]. The velocity of desorption/reaction step is selected to be 3.5 times greater than the feed velocity. 90 % of the purge stream is directed into the adsorber section countercurrently and 10 % is directed into the reactor section cocurrently [Figures 3a,4d]. The waste stream is collected at the interface zone. At the initial part of the cycle, there is a large buildup in velocity due to the desorption of components that were adsorbed in the previous steps [Figure 6d]. The reason for using this 90/10 split is shown in Figure 5 where the purge is 100 % countercurrent. This is a 3 dimensional plot of temperature versus dimensionless bed length and time. In the initial stages of the cycle, the backflow of desorbed normal alkanes is so high that the reactor becomes unstable with a temperature rise to 1,200 °C on entry into the catalytic section where exothermic reaction and adsorption of both iso and normal alkanes takes place. This is unacceptable as the catalyst will be destroyed at these temperatures. Hence, we resorted to splitting the purge in a 90/10 ratio and collecting the product at the interface. In later papers we collect

and recycle this material.

The concentrations of the alkane components at the end of the cyclic steps are illustrated in a 2-dimensional plot in Figure 6 and during the cyclic steps in 3-dimensional plots in Figures 7 to 10. Only the internal collocation points are plotted in all figures as the boundary points are not included. The only exception to this rule is the velocity profiles given earlier. Fresh feed is introduced to the bed with an equivalent molar ratio of 0.03 for each of the reactive components. The molar ratios of reactive components are selected to maintain an overall minimum hydrogen to hydrocarbon ratio of 7.33 which is crucial to limiting any hydrocracking reactions from taking place. All reactive components adsorb in the catalyst bed before reacting during the isomerization equilibrium based reactions. Reactants form products but equilibrium is not approached. In the reaction/pressurization step, the vessel pressure is elevated from 2 to 15 bars in preparation for the next cyclic step. During this step the other end of the vessel is closed. Minimal reaction takes place in this step as components are mainly adsorbed in the Y catalyst [7a, 8a, 9a, 10a]. The isohexane peak appearing towards the end of the adsorber bed is due to the shift of the amounts of isohexane that were present in the interface region at the end of the previous desorption/reaction step.

The gas phase concentrations of reactive components during the reaction /adsorption step is illustrated in the b sections of Figures 7 to 10. In this step, the back end of the vessel is open for product collection. Isomerization of n-C_5 takes place at the first three centimeters of the bed but it takes the entire reactor section length to bring n-C_6 isomerization to its equilibrium state [Figures 7b, 8b]. In the adsorber section, any unreacted n-C_5 and n-C_6 left over from the equilibrium reaction adsorbs on the 5A zeolite pellets. It takes 16 minutes for i-C_5 to breakthrough the reactor section [Figure 9b] and it takes 43 minutes for i-C_6 to breakthrough the reactor section [Figure 10b]. Noticeable amounts of n-C_5 and n-C_6 start appearing at the inlet of the adsorber section during this step [Figures 7b, 8b]. This is due to the pellets at this section reaching their equilibrium occupation. Because of the higher adsorption equilibrium constant for n-C_6 over n-C_5, the amounts of n-C_6 adsorbed are higher than those of n-C_5 [Figures 14a, 14b]. The equilibrium K values favor the adsorption of n-C_6 over n-C_5 displacing adsorbed n-C_5 in the pellets, pushing the n-C_5 front ahead as n-C_5 is desorbed, generating a small peak in n-C_5 gas phase concentration [Figure 6b]. This step is selected to be 50 times longer than the reaction/pressurization time. The choice of the time interval for this step is somewhat arbitrary provided the time is insufficient to allow the adsorption pellets to reach their equilibrium occupation causing n-C_5 or n-C_6 to breakthrough with the product. But, the selected time should be sufficient to allow for i-C_5 and i-C_6 to breakthrough the adsorber section [Figures 9b, 10b].

The gas phase concentrations of reactive components during the blowdown/reaction step is illustrated in the c sections of Figures 7 to 10. The time interval for this step is exactly the same as that of the reaction/pressurization step. In this step, the front end of the vessel is closed and vessel contents are blown out of the vessel from the back end. Blowing vessel contents from the same open end of the previous reaction/adsorption step is contrary to conventional practice. The reason for reversing the conventional practice setup is to avoid high reactants concentrations exiting the adsorber section and entering the reactor section resulting in a very high unstable temperature profile in the interface region [see Figure 5]. This setup allows for a pressure reduction from 15 bars to 2 bars and prepares the vessel for introduction of the purge stream in the next step. The shift in equilibrium, due to pressure decrease, causes large amounts of reactive components present in the solid phase of both sections to escape to the gas phase. The escape of these compounds to the gas phase causes their gas phase concentrations to increase resulting in a large drop in hydrogen concentration [Figure 11], violating the desirable hydrogen/hydrocarbon ratio to inhibit cracking. This indicates that a slower blowdown possibly involving incremental blowdown pressure drop steps with intermediate hydrogen purging should be considered for actual operation. The gas phase concentration of n-C_5 rises to a peak value of 70 % in the adsorber midsection [Figure 6c, 7c], that of n-C_6 is low going from 30% to zero transiting the adsorber [Figures 6c, 8c], and that of i-C_5 and i-C_6 is maximal at about 48% at the adsorber exit due to their nonadsorption on the 5A pellets [Figures 6c, 9c and 10c].

The gas phase concentrations of reactive components during the desorption/reaction step is illustrated in the d sections of Figures 7 to 10. Note that the scale for d is much lower than that in the other plots. In the present model, pure H_2 is used as a purge stream. The desorption of n-C_5 and n-C_6 amounts present in the solid phase of the adsorber section causes a slight increase in their gas phase concentrations. As indicated earlier, to avoid temperature spike, the purge stream is introduced at both ends of the vessel and the waste

stream is collected from the interface zone. Although, cocurrent desorption avoids temperature spikes, it does not allow for good purge of n-C_5 and n-C_6 from the reactor section [Figure 6d]. This is due to the low fraction of purge used in the reactor section. The gas phase concentrations of n-C_5 and n-C_6 in the adsorber section at cycle end are satisfactory [Figure 6d]. Limited reaction takes place in this step because components in the reaction zone are close to their equilibrium conversions.

The gas phase concentration of hydrogen during the four cyclic steps is illustrated in Figures 11. The concentration is generally above 90% except for the blowdown step where it drops to about 3%. During blowdown step, the pressure reduces from 15 bars to 2 bars causing an equilibrium shift for the components present in the solid phase of both sections. The equilibrium shift causes the amounts initially present in the solid phase to desorb to the gas phase producing a large decrease in the gas phase hydrogen concentration [Figure 11]. During desorption/reaction step, pure hydrogen is used as a purge stream and the concentration of hydrogen rises again to its normal value.

The temperature profiles during the four cyclic steps are illustrated in Figures 12 and 13. The noticeable increase of the temperature at the start of the reactor bed [Figures 12, 13a] during reaction/pressurization step, is due to the combined effects of adsorption and chemical reactions. Temperature constancy through the remainder of the reactor bed is due to a limitation of both of these terms, due to the absence of significant reaction in the remaining portion of the reactor section. A small temperature peak occurs in the adsorber due to the exothermic adsorption of n-C_5 and n-C_6 during the adsorption step. A significant temperature drop to 279°C is noticed in the reactor section during blowdown/reaction step due to energy requirements to desorb the reactive components from the solid phase to the gas phase. As expected an endothermic temperature decrease occurs in the front end of the adsorber but surprisingly a large 20 °C exothermic temperature peak occurs in the rear end of the adsorber during blowdown due to the displacement of n-C_6 towards the adsorber exit [Figure 12 and 13c]. The solid phase profiles are illustrated in Figure 14 consistent with the gas phase description given above.

Table 1: Data for the adsorber section

Adsorbent Properties	
• ρ_b	$= 0.77$ g/cm^3
• ρ_s	$= 1.13$ g/cm^3
• ε	$= 0.32$
• ε_p	$= 0.35$
• d_p	= 1.6 mm
• a_p	= 25 cm^{-1}
Adsorption Equilibrium Isotherm Parameters	
• n-Pentane	
K_o	$= 2.013 * 10^{-5}$ bar^{-1}
$-\Delta H_{adsorption}$	$= 13.2$ kcal/mol
q_{max}	$= 13.0$ g/100g
n	$= 5$
• n-Hexane	
K_o	$= 4.9187 * 10^{-5}$ bar^{-1}
$-\Delta H_{adsorption}$	$= 14.2$ kcal/mol
q_{max}	$= 13.0$ g/100g
n	$= 6$

Table 2: Reaction & Adsorption Parameters for Reactor Section

Reaction Parameters	
• n-Pentane $k_o = 9.4657*10^7$ s^{-1} $\Delta H_{Reaction} = -22.0*10^3$ (cal/gmol) $K_C = 3.310$	• n-Hexane $k_o = 3.472*10^9$ s^{-1} $\Delta H_{Reaction} = -31.6*10^3$ (cal/gmol) $K_C = 2.865$
Adsorption Parameters	
• n- Pentane $K_o = 6.46*10^{-10}$ bar^{-1} $-\Delta H_{Adsorption} = 17.0*10^3$ (cal/gmol) $q_{max} = 13.92$g/100g $n = 3$	• n-Hexane $K_o = 2.44*10^{-12}$ bar^{-1} $-\Delta H_{Adsorption} = 20.5*10^3$ (cal/gmol) $q_{max} = 14.48$g/100g $n = 4$
• i- Pentane $K_o = 6.46*10^{-10}$ bar^{-1} $-\Delta H_{Adsorption} = 17.0*10^3$ (cal/gmol) $q_{max} = 13.65$g/100g $n = 3$	• i-Hexane $K_o = 2.44*10^{-12}$ bar^{-1} $-\Delta H_{Adsorption} = 20.5*10^3$ (cal/gmol) $q_{max} = 14.48$g/100g $n = 4$

Table 3: Parametric Values used for simulation of PSAR systems

Parameter	Value	Parameter	Value
yAf = yBf = yCf = yDf	0.03	DL @ high pressure (cm2/s)	0.088
H2/HC ratio (mol/mol)	7.33	DL @ low pressure (cm2/s)	0.66
Ff (mol/m2/s)	0.134	Kgl @ high pressure (cm/s)	0.62
PH (bar)	15	Kgl @ low pressure (cm/s)	2.23
PL (bar)	2	Pe @ high pressure	59.1
Tf (K)	573	Pe @ low pressure	7.87
L (cm)	110	θ Aref ,1@ 573K	0.0541
D (cm)	12.7	θ Bref ,1@ 573K	0.1187
Uf (cm/s)	0.5	θ C,ref,1 @ 573K	0.0541
Purge/Feed volumetric ratio	3.5	θ D,ref,1 @ 573K	0.1187
S Reactor Section Purge Velocity Ratio	0.1	θ Aref ,2@ 573K	0.0844
Pressurization & Blowdown time (min)	3.67	θ Bref ,2@ 573K	0.3036
Adsorption & Desorption time (min)	165	ω	0.58

4 CONCLUSIONS

The nonisothermal reaction and separation of 5 components: n-pentane, n-hexane, iso-pentane, isohexane and hydrogen in a PSAR unit is modeled. Countercurrent blowdown and desorption is not used due to the high concentrations of normal alkanes desorbing from the solid to the gas phase in the adsorber section, and subsequently reacting rapidly to form products in the reactor. Due to their high concentrations, the reaction releases sufficient energy to cause a reaction runaway involving a large temperature peak of 1200 °C at the interface region. Consequently, the blowdown step is co-current and the desorption purge step is split 10 % co-current through the reactor bed and 90 % countercurrent through the adsorption bed. The 'waste' stream exits at the interface of the reactor and adsorber. In subsequent studies this is reused.

Modeling of the system provided insight into the difficulties of the process. Three dimensional plots revealed problems not discovered through 2D end of stage cyclic plots. A runaway 1200°C temperature peak is observed in the 3D plotting of temperature profile against time and space and not in the 2D plots.

5 REFERENCES

1 Vaporciyan, G. G., and R. H. Kadlec, "Equilibrium Limited Periodic Separating Reactors," AlChEJ., 33, 1334 (1987).

2 Vaporciyan, G. G., and R. H. Kadlec, "Periodic Separating Reactors: Experiments and Theory," AlChE J., 3, 831 (1989).

3 Morbidelli, M., M. Mazzotti, R. Baciochi, and G. Storti, "Vapor-Phase SMBAdsorptive Separation of Linear/Nonlinear Paraffins," Ind. Eng. Chem. Res.. 35, 2313 (1996).

4 Alplay, E., D. Chatsiriwech, L. S. Kershenbaum, C. P. Hull, and N. F. Kirby, "Combined Reaction and Separation by Pressure Swing Adsorption," Chem. Eng. Sci., 49, 5845-5864 (1995).

5 Alplay, E., Y. S. Cheng, and L. S. Kershenbaum, "Simulation and Optimization of a Rapid Pressure Swing Reactor," Comp. Chem. Eng., 22, S45-S52 (1998).

6 Arumugam, B. K., Wankat, P.C., "Pressure Transients in Gas Phase Adsorptive Reactors", Adsorption, 4, 345-354 (1998.

7 Kodde, A. J., Fokma, Y. S., Bliek, A., "Selectivity Effects on Series of Reactions by Reactant Storage and PSA Operation", AIChEJ, 46(11), 2295-2305 (2000).

8 Xiu, G. H., Li, P., Rodrigues, A. E., "New Generalized Strategy for Improving Sorption-Enhanced Reaction Process", Chem. Eng. Sci, 58, 3425-3437 (20030

9 Hufton, J. R., Mayorga, S., Sircar, S., "Sorption-Enhanced Reaction Process for Hydrogen Production", 45(9), 248-255 (1999).

10 Al-Juhani, A.A., Loughlin, K.F., "Simulation of a Combined Isomerization Reactor and Pressure Swing adsorption Unit", Adsorption, 9, 251-264 (2003).

11 Elsner, M. P., Dittrich, C., Agar, D. W., "Adsorptive Reactors for Enhancing Equilibrium Gas-Phase Reactions – Two Case Studies", Chem. Eng. Sci., 57(9), 1607-1619 (2002).

12 Sircar, S., B. T. Carvill, J. R. Hufton, and M. Anand, "Sorprion-Enhanced Reaction Process," AlChEJ., 42(10), 2765-2772 (1996).

13 Bryant, P. and J. V. Spivey, "Hydroisomerization of n-C_5 and n-C_6 Mixtures on Zeolite Catalysts," *Ind. Eng. Chem. Proc. Des. Dev.*, 21(4), 750-760 (1982).

14 Morbidelli, M., A. Servida, and G. Storti, "Simulation of Multicomponent Adsorption Bed- Model Analysis and Numerical Solution," Ind. Eng. Chem. Fundam., 21, 123 (1982).

15 Nitta, Tomoshige, Masayuki Kuro-Oka, and Takashi Katayama, "An Adsorption Isotherm of Multi-site Occupancy Model for Homogeneous Surface," J. Chem.Eng. Jpn., 17, 39-45 (1984).

16 Silva, J, A., and A. E. Rodrigues, "Sorption and Diffusion of n-Pentane in Pellets of 5A Zeolite," Ind. Eng. Chem. Res., 36, 493-500 (1997).

17 Silva, J. A., and A. E. Rodrigues. "Equilibrium and Kinetics of n-Hexane Sorption in Pellets of 5A Zeolite," AlChE J., 43, 2524-2534 (1997).

18 Barrer, R. M. and J. W. Sutherland, "Inclusion complexes of faujasite with paraffins and permanent gases," Physical Chemistry Laboratories, Imperial College, London, 1956.

19 Al-Soudani, Tareg M., "Modeling and Simulation of a Combined Isomerization Reactor/Pressures Swing Adsorption/Membrane Unit", M.S. thesis, King Fahd University of Petroleum & Minerals, June 2004.

ACKNOWLEDGMENTS

The authors wish to acknowledge the support of King Fahd University of Petroleum & Minerals, Dhahran, Saudi Arabia during the course of this work.

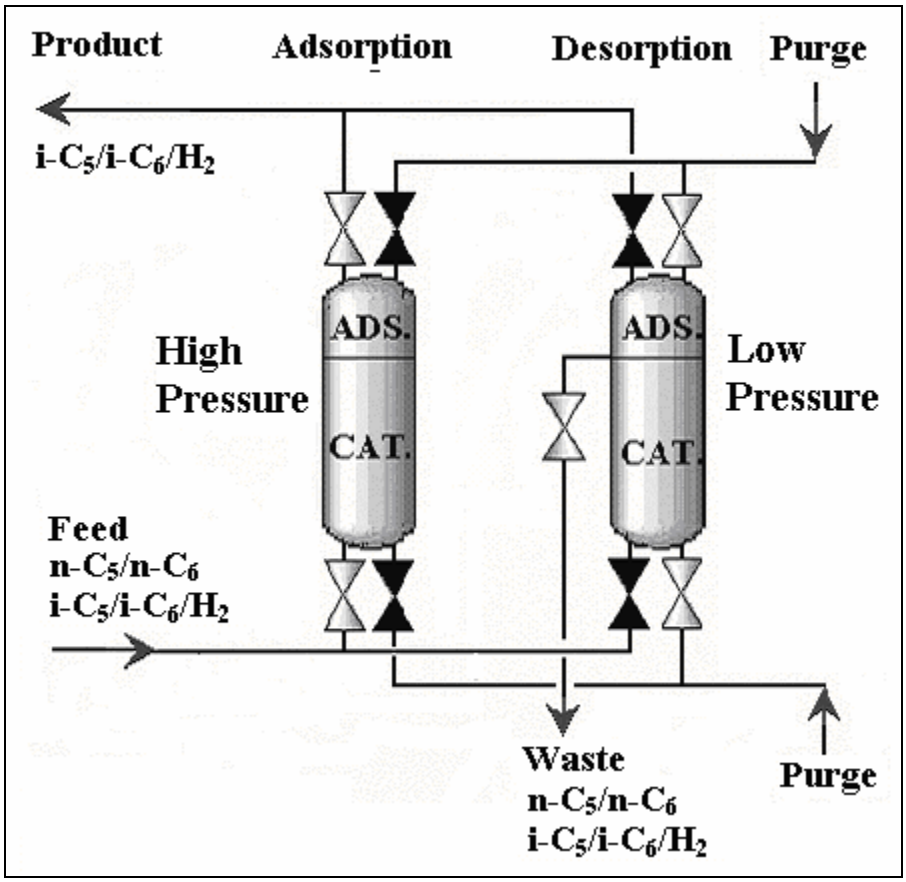

Figure 1: Flow diagram for the Combined Isomerization Reactor/Adsorber process.

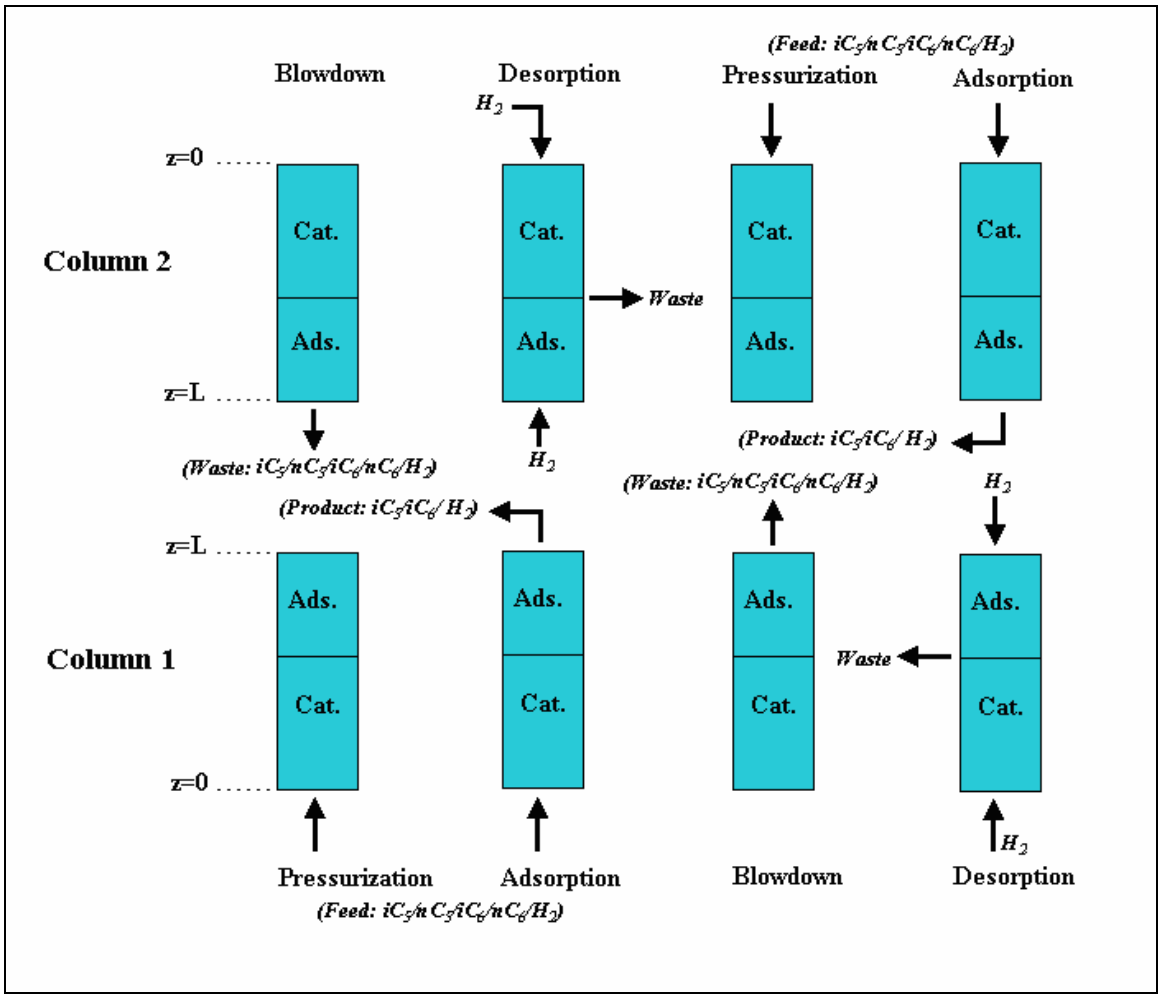

Figure 2: Proposed cyclic steps for PSAR unit.

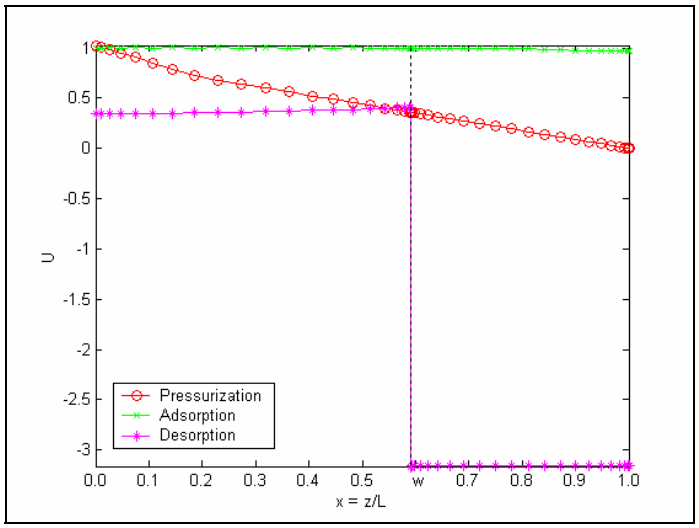

a.

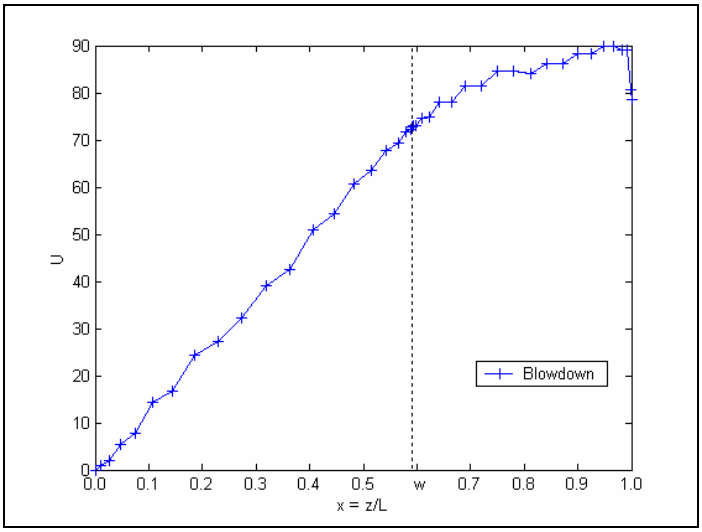

b.

Figure 3: Velocity Profiles in the bed at the end of cyclic steady state:

a. Pressurization, Adsorption and Desorption steps Profiles.
b. Blowdown step profile.

Parametric values are in Table 3. (Conventional PSAR unit/H_2 purge).

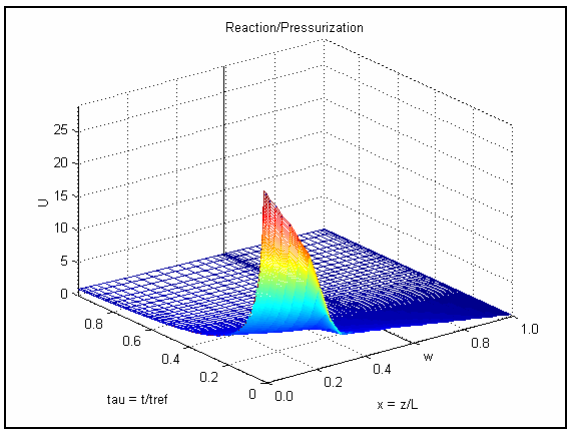

a. Reaction/Pressurization

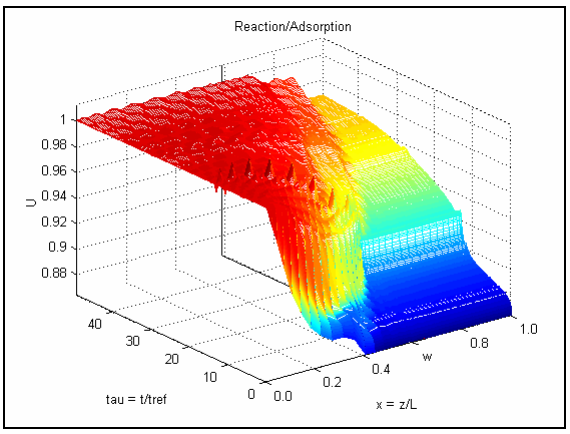

b. Reaction/Adsorption

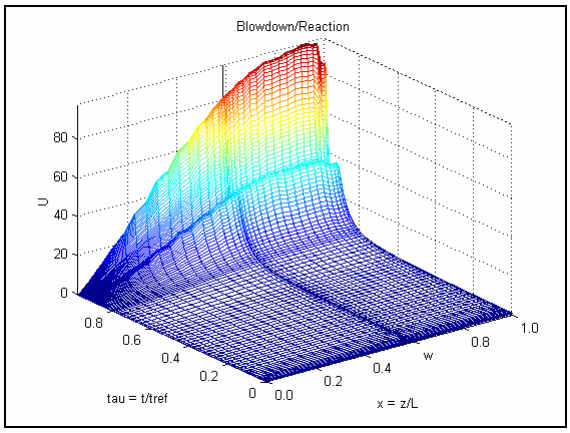

c. Blowdown/Reaction

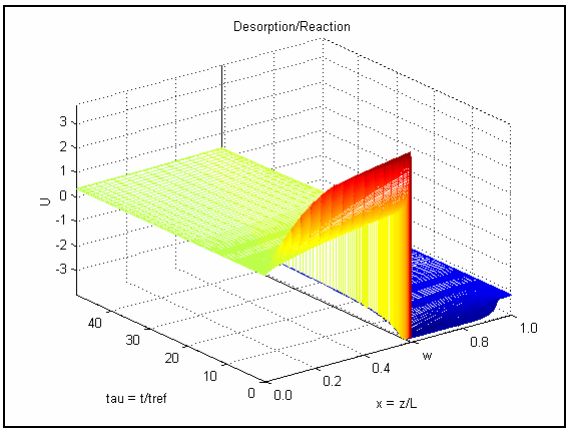

d. Desorption/Reaction

Figure 4: Three dimensional drawing illustrating the transient and spatial change in Velocity with respect to time and axial distance for the four basic steps at the steady state cycle. (Conventional PSAR Unit/Hydrogen Purge)

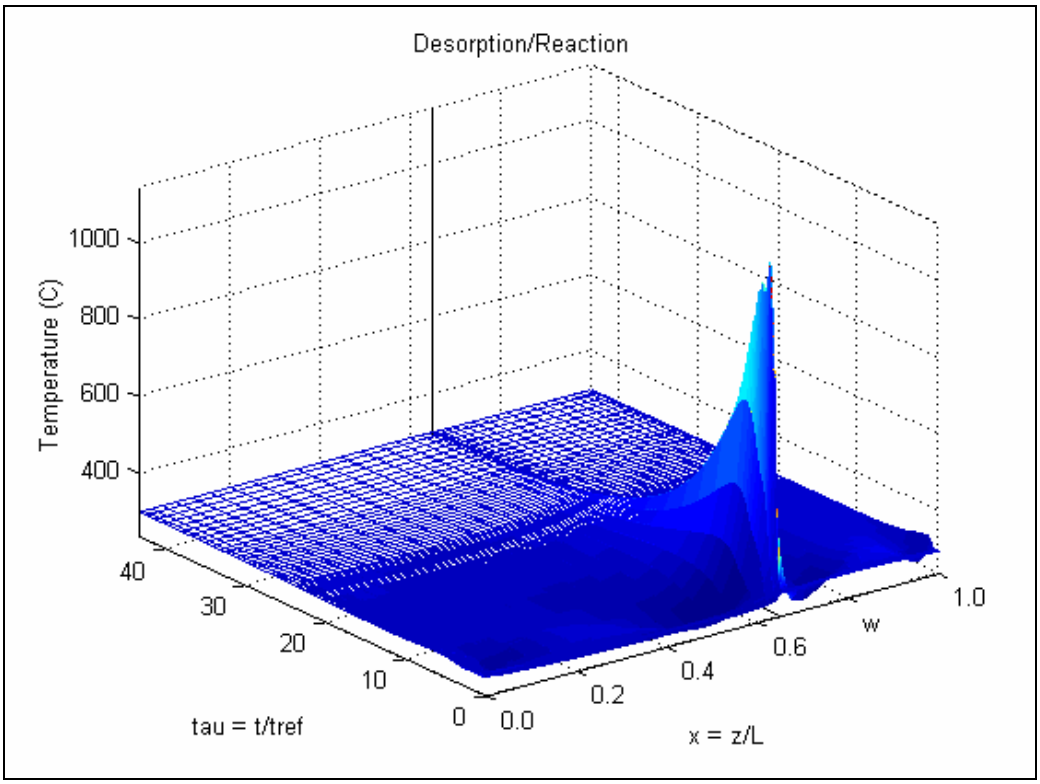

Figure 5: Three dimensional drawing illustrating the transient and special change in Temperature with respect to time and axial distance for counter current desorption.

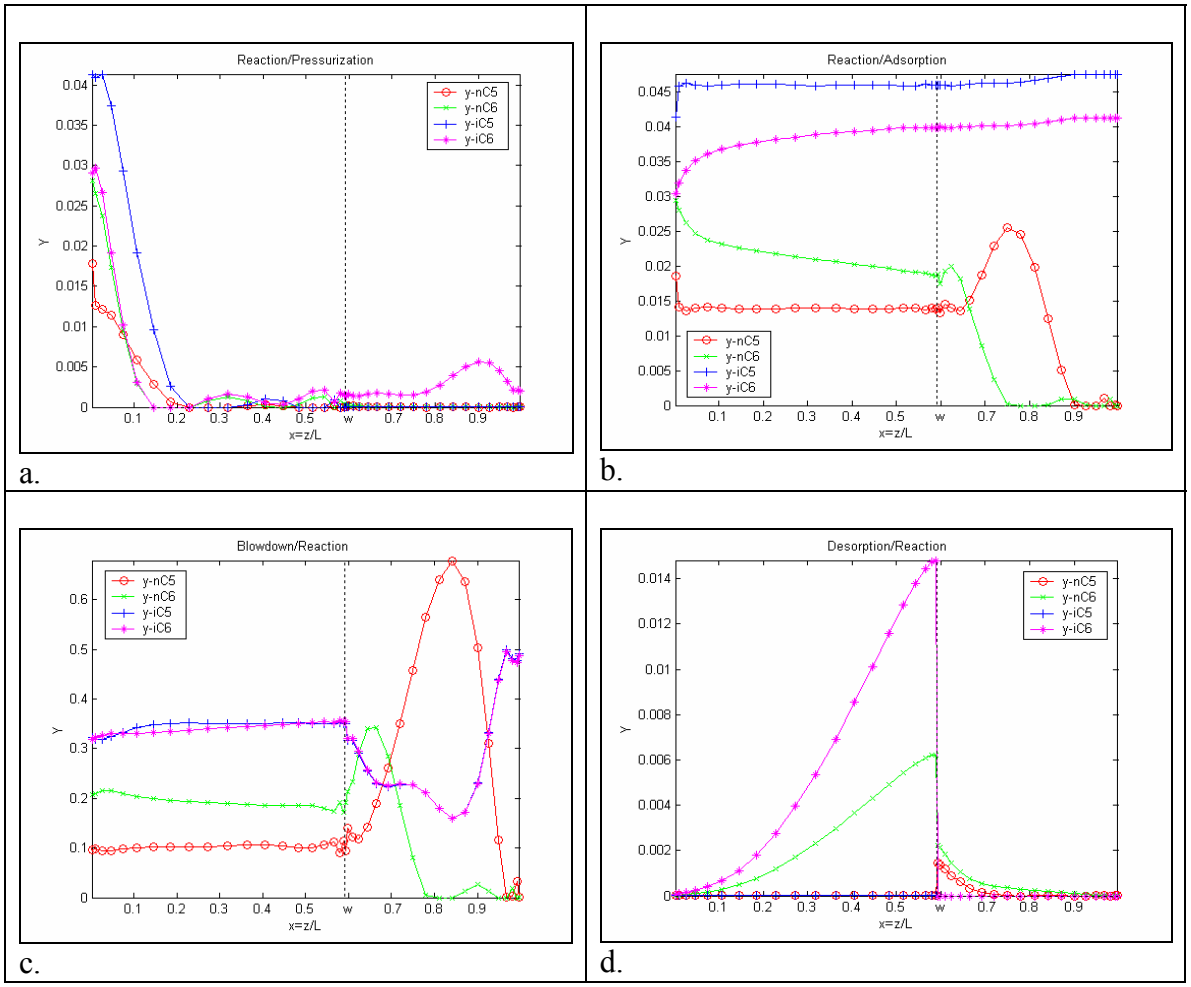

Figure 6: Gas phase concentration profiles for reactive components in the PSAR bed at the end of cyclic steady state:

a.) reaction/pressurization,
b.) reaction/adsorption,
c.) blowdown/reaction,
d.) desorption/reaction.

Parametric values are in Table 3. (Conventional PSAR unit/H_2 purge).

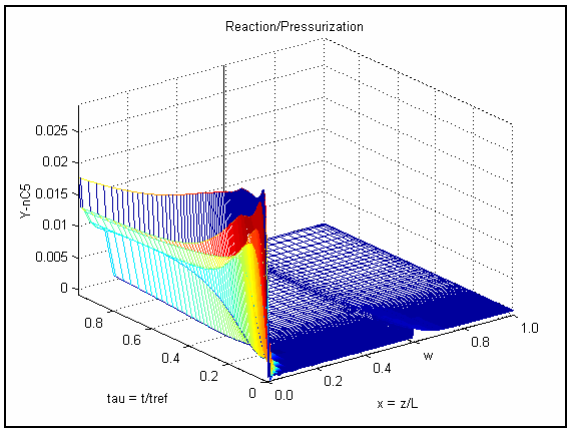

a. Reaction/Pressurization

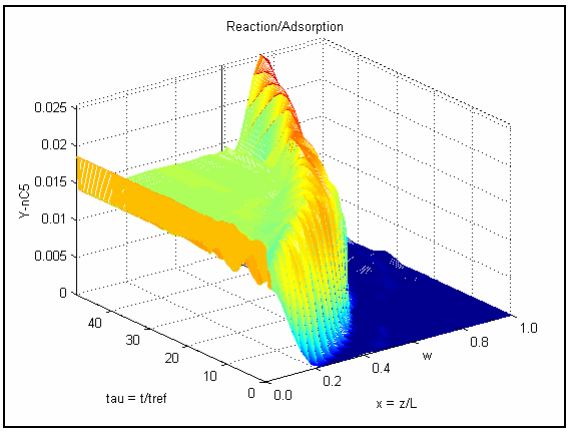

b. Reaction/Adsorption

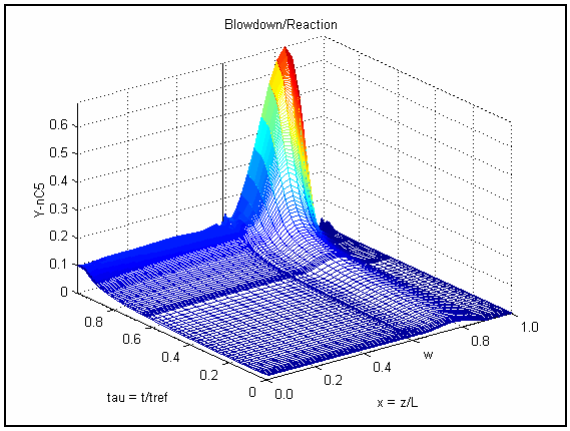

c. Blowdown/Reaction

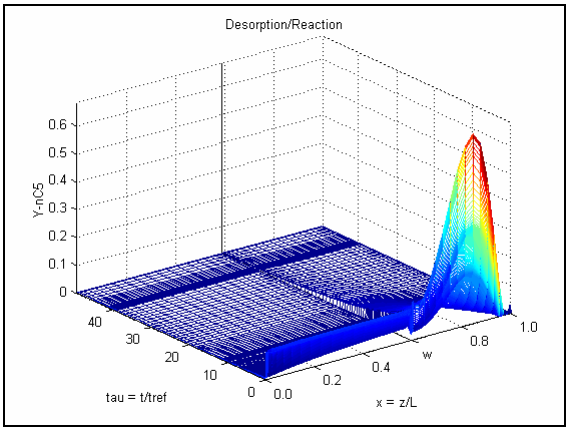

d. Desorption/Reaction

Figure 7: Three dimensional drawing illustrating the transient and spatial change in n-C_5 concentration with respect to time and axial distance for the four basic steps at the steady state cycle. (Conventional PSAR Unit/Hydrogen Purge)

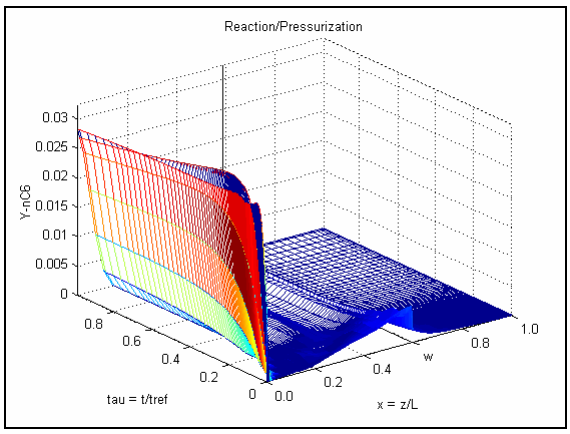

a. Reaction/Pressurization

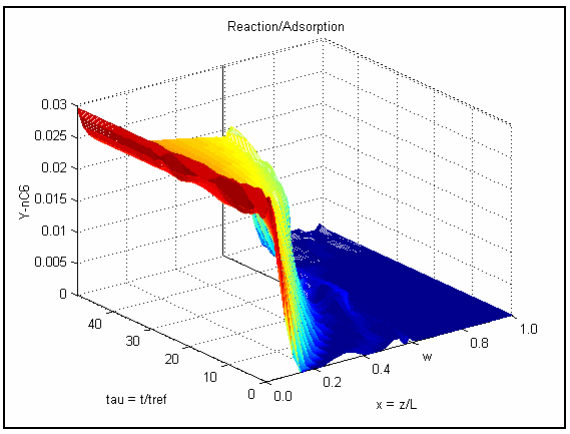

b. Reaction/Adsorption

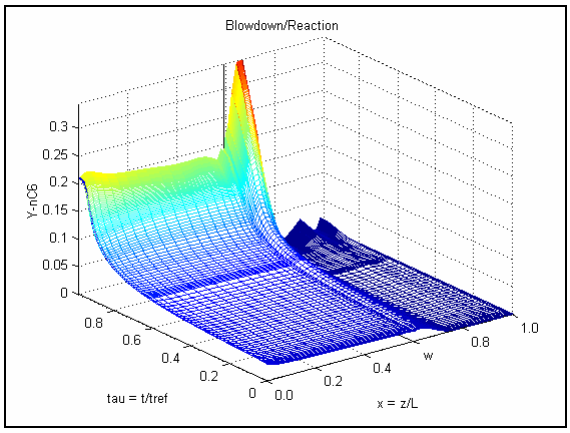

c. Blowdown/Reaction

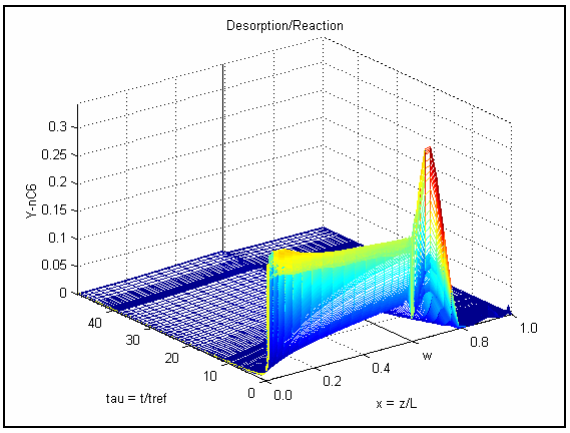

d. Desorption/Reaction

Figure 8: Three dimensional drawing illustrating the transient and spatial change in n-C_6 concentration with respect to time and axial distance for the four basic steps at the steady state cycle. (Conventional PSAR Unit/Hydrogen Purge)

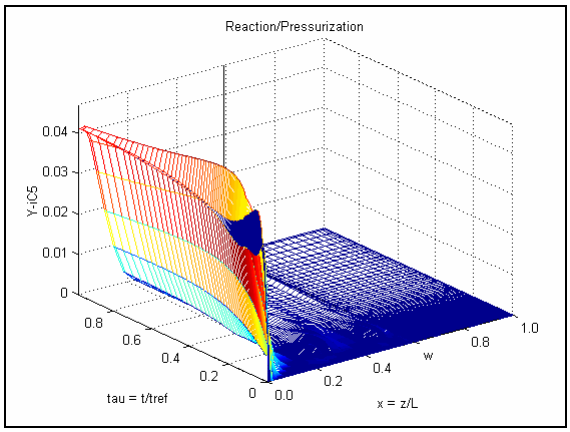

a. Reaction/Pressurization

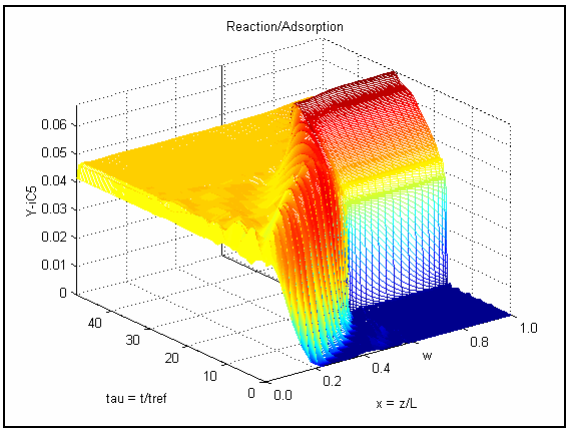

b. Reaction/Adsorption

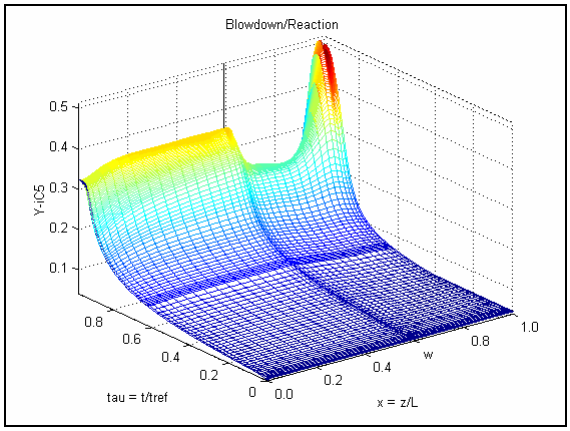

c. Blowdown/Reaction

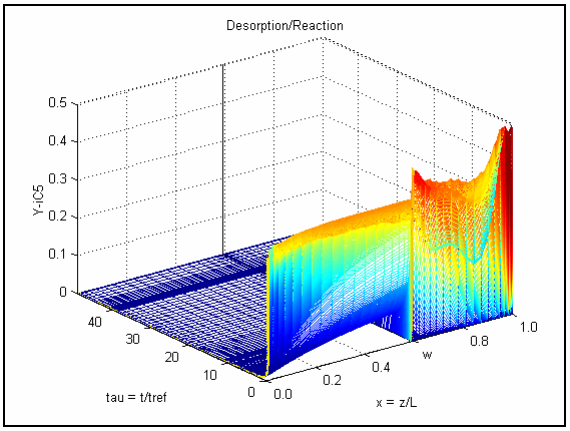

d. Desorption/Reaction

Figure 9: Three dimensional drawing illustrating the transient and spatial change in i-C_5 concentration with respect to time and axial distance for the four basic steps at the steady state cycle. (Conventional PSAR Unit/Hydrogen Purge)

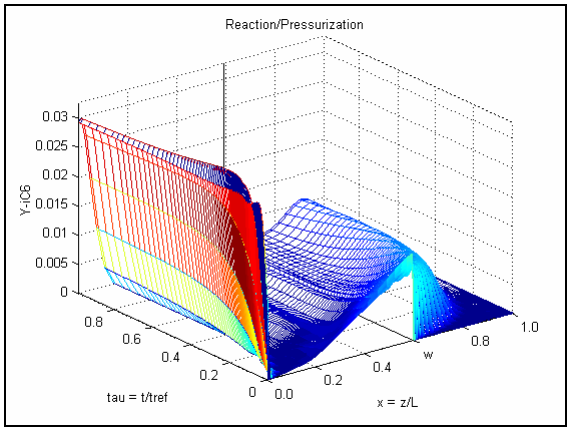

a. Reaction/Pressurization

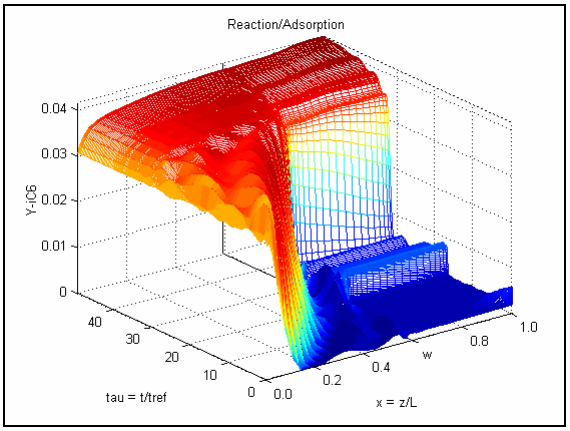

b. Reaction/Adsorption

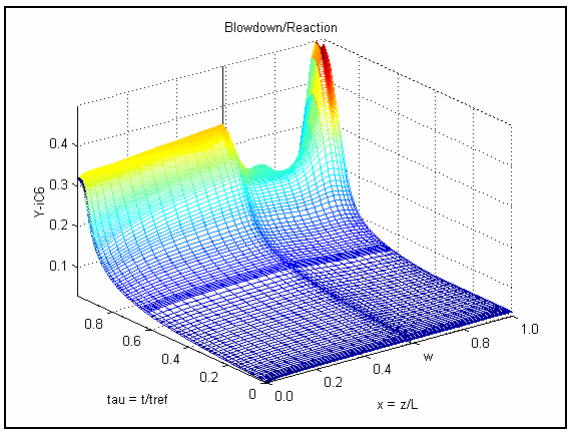

c. Blowdown/Reaction

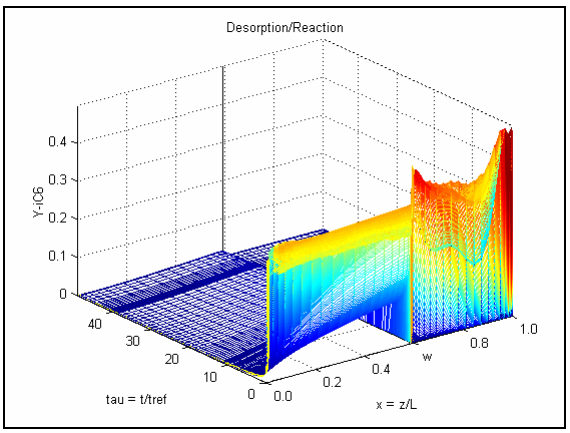

d. Desorption/Reaction

Figure 10: Three dimensional drawing illustrating the transient and spatial change in i-C_6 concentration with respect to time and axial distance for the four basic steps at the steady state cycle. (Conventional PSAR Unit/Hydrogen Purge)

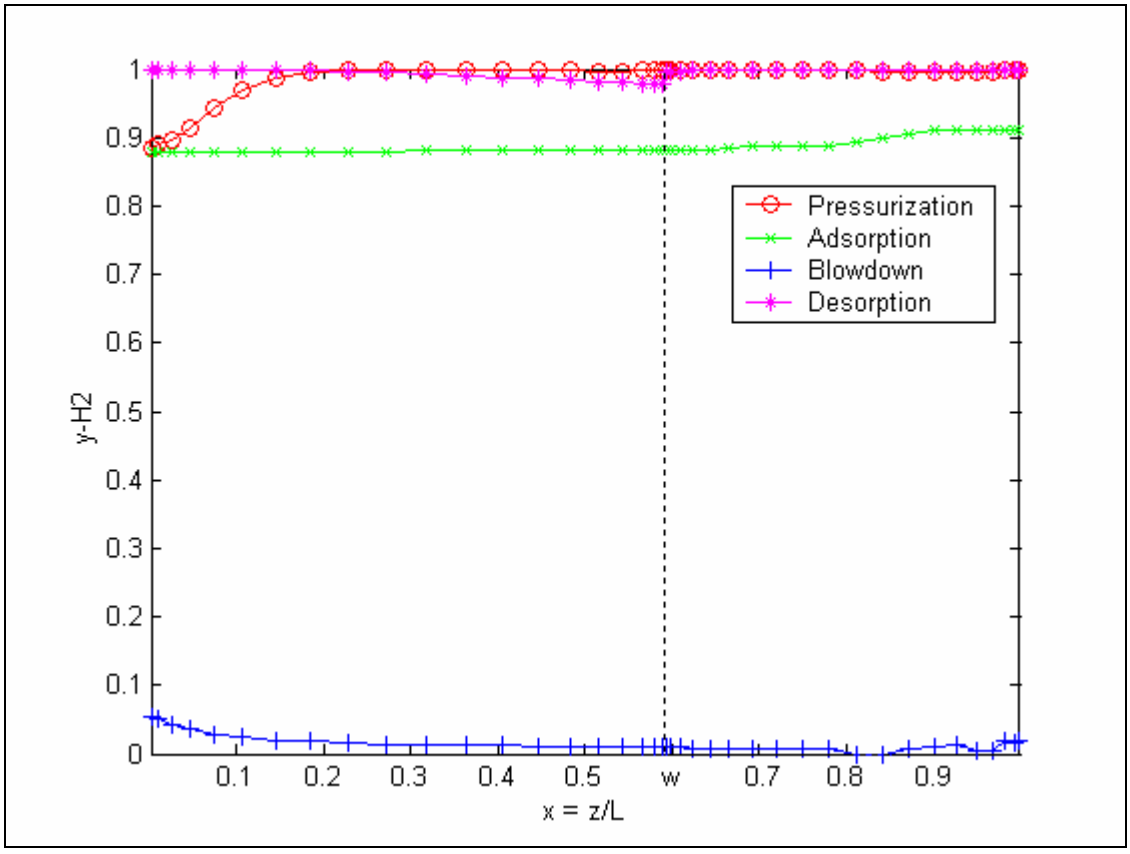

Figure 11: Gas phase concentration profiles for H_2 in the PSAR bed at the end of cyclic steady state. Parametric values are in Table 3. (Conventional PSAR unit/H_2 purge).

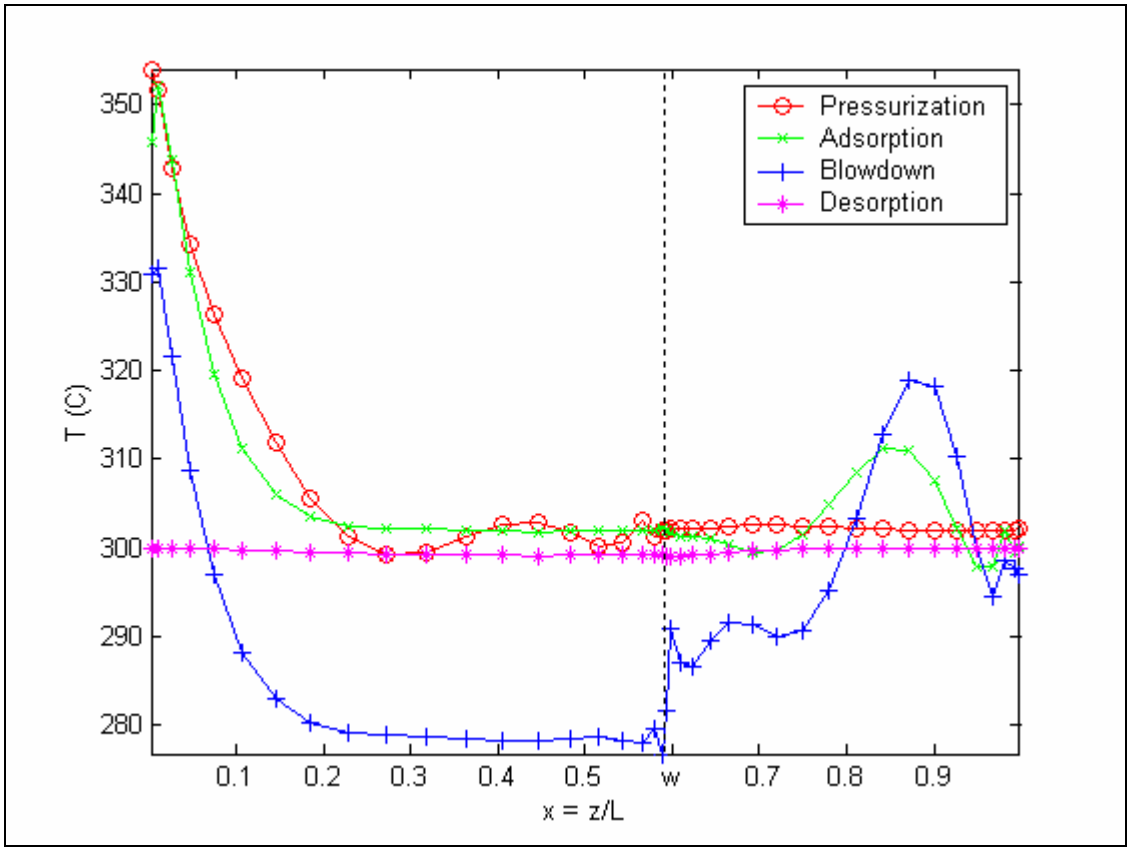

Figure 12: Temperature Profiles in the bed at the end of cyclic steady state. Parametric values are in Table 3. (Conventional PSAR unit/H_2 purge).

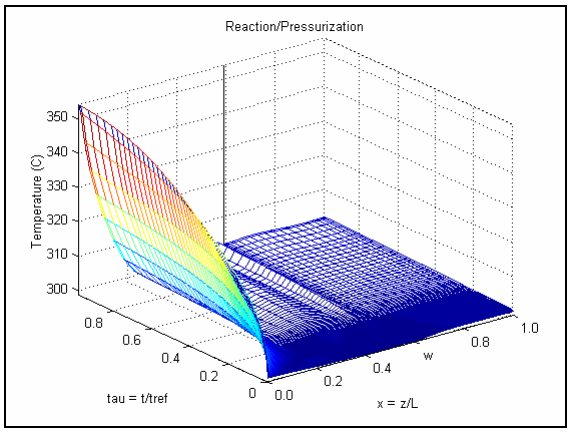

a. Reaction/Pressurization

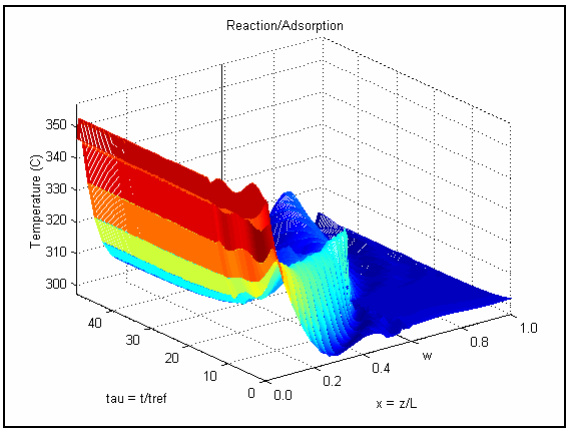

b. Reaction/Adsorption

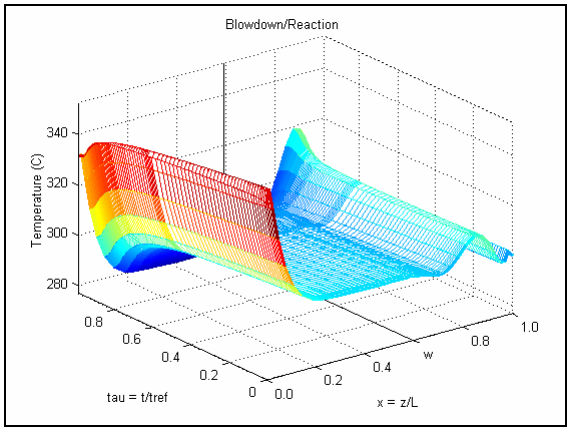

c. Blowdown/Reaction

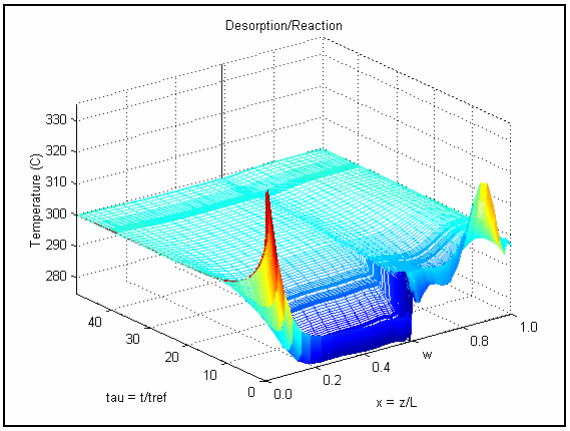

d. Desorption/Reaction

Figure 13: Three dimensional drawing illustrating the transient and spatial change in Temperature with respect to time and axial distance for the four basic steps at the steady state cycle. (Conventional PSAR Unit/Hydrogen Purge)

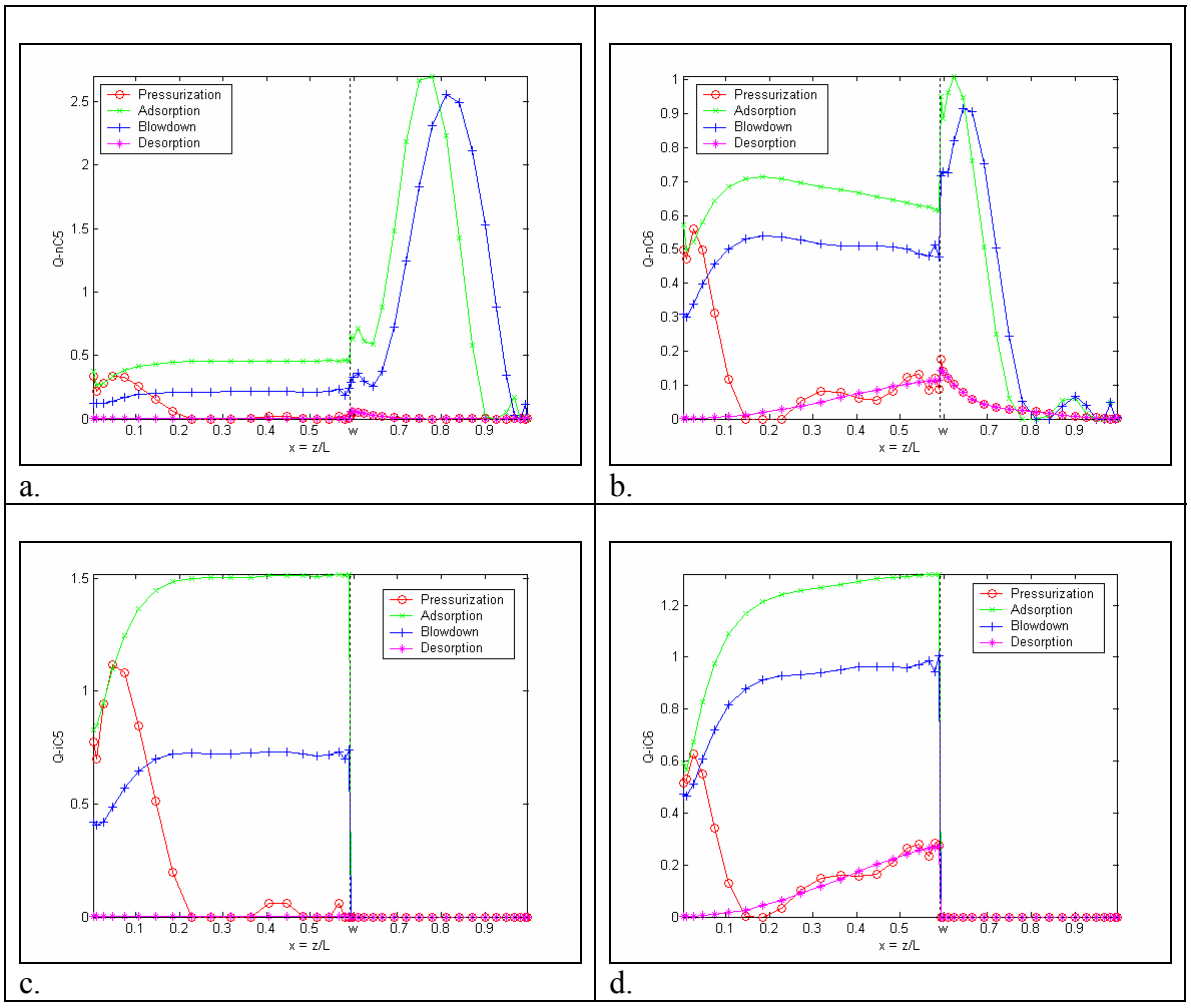

Figure 14: Solid phase capacitance profiles for reactive components in the PSAR bed at the end of cyclic steady state:
a.) n-C_5,
b.) n-C_6,
c.) i-C_5,
d.) i-C_6
Parametric values are in Table 3. (Conventional PSAR unit/H_2 purge).